
DUETSERVE: HARMONIZING PREFILL AND DECODE FOR LLM SERVING VIA ADAPTIVE GPU MULTIPLEXING

Lei Gao¹ Chaoyi Jiang¹ Hossein Entezari Zarch¹ Daniel Wong² Murali Annavaram¹

ABSTRACT

Modern LLM serving systems must sustain high throughput while meeting strict latency SLOs across two distinct inference phases: compute-intensive prefill and memory-bound decode phases. Existing approaches either (1) aggregate both phases on shared GPUs, leading to interference between prefill and decode phases, which degrades time-between-tokens (TBT); or (2) disaggregate the two phases across GPUs, improving latency but wasting resources through duplicated models and KV cache transfers. We present DuetServe, a unified LLM serving framework that achieves disaggregation-level isolation within a single GPU. DuetServe operates in aggregated mode by default and dynamically activates SM-level GPU spatial multiplexing when TBT degradation is predicted. Its key idea is to decouple prefill and decode execution only when needed through fine-grained, adaptive SM partitioning that provides phase isolation only when contention threatens latency service level objectives (SLOs). DuetServe integrates (1) an attention-aware roofline model to forecast iteration latency, (2) a partitioning optimizer that selects the optimal SM split to maximize throughput under TBT constraints, and (3) an interruption-free execution engine that eliminates CPU–GPU synchronization overhead. Evaluations show that DuetServe improves total throughput by up to 1.3x while maintaining low generation latency compared to state-of-the-art frameworks.

1 INTRODUCTION

Large Language Models (LLMs) have unlocked unprecedented capabilities, powering applications such as conversational assistants (OpenAI et al., 2024a; Gemini-Team et al., 2024), autonomous agents (Li et al., 2023; Luo et al., 2025), and creative content generation (OpenAI et al., 2024b; Liu et al., 2024). User requests in these systems are served in real time by large GPU clusters in the cloud. As these systems scale to millions of concurrent sessions, ensuring efficient use of GPU resources while meeting strict Service Level Objectives (SLOs) for real-time responses becomes increasingly difficult—fast response times typically require over-provisioning system resources.

The key hardware resources involved include the GPU’s high-bandwidth memory (HBM) capacity, memory bandwidth, and streaming multiprocessors (SMs). LLM inference consists of two distinct phases with different resource requirements: (1) the *prefill* phase, which encodes the input prompt in a single forward pass and is highly compute-intensive; and (2) the *decode* phase, which generates output tokens iteratively, performs lightweight per-step computations, and is constrained mainly by memory bandwidth and

capacity. Due to the autoregressive nature of LLM inference, repeated computation of key (K) and value (V) matrices can be avoided by using KV caches that store intermediate attention states. However, storing and repeatedly reading the KV cache during decoding places significant pressure on HBM capacity and memory bandwidth.

The prefill and decoding speed directly impact two key LLM serving metrics: Time-to-First-Token (TTFT), the delay before producing the first output token, and Time-Between-Tokens (TBT), the latency between successive output tokens. TTFT is dominated by the prefill phase, while TBT is determined by the decode phase. Reducing TTFT and TBT typically requires using smaller batch sizes, as batch size directly affects compute and memory usage. In contrast, improving resource utilization and throughput (measured in tokens/sec or requests/sec) benefits from larger batch sizes. Balancing this tradeoff is central to scaling online serving systems efficiently.

A variety of techniques have been proposed to balance throughput and latency (both TTFT and TBT) (Yu et al., 2022; Kwon et al., 2023; Dao et al., 2022; Agrawal et al., 2024b; Zheng et al., 2024). The simplest, *request-level batching*, groups multiple requests into a single batch that runs to completion before admitting the next batch. This approach maximizes throughput when each request has similar, predictable latency, as in conventional DNN inference workloads. However, in LLM serving, where autoregres-

¹University of Southern California, Los Angeles, California, USA ²University of California, Riverside, California, USA. Correspondence to: Lei Gao <leig@usc.edu>.

sive decoding leads to highly variable per-request runtimes, this method is inefficient. A major advance is *continuous batching* (Yu et al., 2022), which performs iteration-level scheduling by dynamically adding or removing requests from the batch at each generation step. This allows shorter requests to complete without waiting for longer ones, improving GPU utilization and reducing queuing delay.

In continuous batching, prefill and decode requests are executed synchronously within each iteration. When long prefill requests are inserted into ongoing decode batches, they can cause unbounded TBT inflation. To mitigate this, Sarathi-Serve (*chunked prefill*) (Agrawal et al., 2024b) introduces a token-budget-based scheduling policy. Their approach assumes that model latency is dominated by linear layers and treats each token, whether from prefill or decode, as contributing equally to computational cost. The scheduler selects a batch whose total token count saturates the “knee” of the linear layer’s roofline curve. Decode requests consume one token from the budget, while a prefill request consumes as many tokens as its prompt length. Prefill requests are admitted as long as the remaining budget can accommodate their full prompt; otherwise, they are chunked to fill the remaining token budget exactly. This design effectively bounds iteration latency while maintaining high GPU utilization.

As discussed in Section 3, with the rapid growth of GPU compute capability, the optimal token budget has increased from 2048 on A100 to 8192 on H100. Fully utilizing compute resources now requires batching many more prefill and decode requests. However, batching such heterogeneous workloads can cause interference between prefill and decode operations, prolonging iteration latency and violating TBT SLOs. Moreover, the token-budget-based design assumes that linear layers dominate model latency, which is not always true, especially for requests with long input contexts, where attention operations become the primary bottleneck in both prefill and decode. Consequently, scheduling decisions based on this assumption can be inaccurate and suboptimal, as shown in Section 3.

To eliminate prefill–decode interference, recent systems have explored disaggregation, which assigns prefill and decode workloads to separate GPU clusters and transfers KV caches between them (Zhong et al., 2024; Patel et al., 2024; Qin et al., 2025). Disaggregation enables phase-specific optimizations, such as distinct parallelization strategies (tensor, pipeline, etc.), but introduces new challenges, such as (1) additional communication overhead from KV cache transfer, (2) reduced effective KV cache capacity due to duplicated model weights and non-shared GPU memory, and (3) hardware underutilization caused by workload imbalance between clusters, which worsens under dynamic and skewed traffic. For example, more incoming requests

may overload prefill servers, while longer output contexts may saturate decode servers.

The key challenge is to achieve disaggregation-level performance isolation only when necessary, without permanently incurring its overhead. To this end, we introduce **Duet-Serve**, an adaptive serving framework that operates in an aggregated mode by default and dynamically enables GPU spatial multiplexing when an SLO violation, particularly a TBT degradation, is predicted. The key idea of DuetServe is to decouple prefill and decode execution *within a single GPU* through fine-grained SM-level partitioning, providing phase isolation only when contention threatens latency SLOs. Leveraging modern GPU capabilities, the system logically partitions hardware resources within a single device by dividing GPU SMs into distinct, concurrently executing sets. These logical “sub-GPUs” isolate prefill and decode workloads during periods of interference and revert to fully shared execution when contention subsides, maintaining both high throughput and low latency.

Our contributions are as follows. DuetServe consists of three tightly integrated components: (1) an attention-aware roofline analytical model that predicts iteration latency based on operator-level compute and memory characteristics, allowing the scheduler to detect potential TBT violations in advance; (2) a dynamic GPU partitioning optimizer that determines the optimal allocation of SMs between prefill and decode to balance utilization and latency, activating GPU spatial multiplexing only when necessary; and (3) an interruption-free execution engine that employs look-ahead decode scheduling and asynchronous kernel dispatch to eliminate CPU–GPU synchronization overhead and ensure uninterrupted concurrent execution. (4) We evaluate Duet-Serve on Qwen3-8B and Qwen3-14B using three realistic workloads and show up to 1.3× total throughput improvement while maintaining low TBT latency compared to the state-of-the-art LLM serving frameworks.

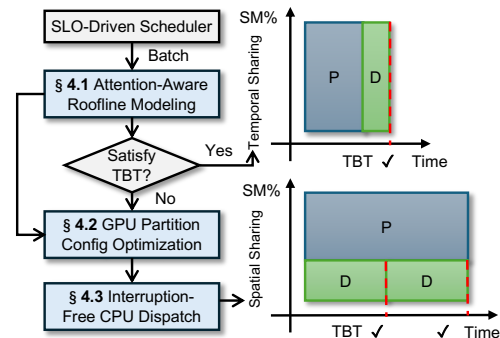


Figure 1. Overview of DuetServe.

2 BACKGROUND

LLM Inference Process. Let $x \in \mathbb{R}^{s \times d}$ denote a single input request, where s is the sequence length (i.e., the number of prompt tokens) and d is the embedding dimension. The forward pass of a Transformer block in typical LLMs such as Qwen (Yang et al., 2025) and Llama (Grattafiori et al., 2024) can be expressed as:

$$\begin{aligned} Q &= xW_q, \quad K = xW_k, \quad V = xW_v, \quad W_{q,k,v} \in \mathbb{R}^{d \times d}, \\ u &= \text{Softmax}\left(\frac{QK^\top}{\sqrt{d}}\right)VW_o, \quad W_o \in \mathbb{R}^{d \times d}, \\ v &= \text{LayerNorm}(u + x; \gamma_1, \beta_1), \quad \gamma_1, \beta_1 \in \mathbb{R}^d, \\ z &= \sigma(vW_1)W_2, \quad W_1, W_2^T \in \mathbb{R}^{d \times m}, \\ y &= \text{LayerNorm}(z + u + x; \gamma_2, \beta_2), \quad \gamma_2, \beta_2 \in \mathbb{R}^d. \end{aligned}$$

During the prefill phase, the generated K and V matrices are stored in the KV cache. In the decode phase, the decoder layer processes one token at a time, with the input $x \in \mathbb{R}^{1 \times d}$. The KV cache is updated by concatenating the newly computed key and value pairs with the existing ones before the attention operation:

$$K = \text{concat}(K, xW_k), \quad V = \text{concat}(V, xW_v).$$

The rest of the operations in the decoding phase are identical to those in the prefill phase.

GPU Spatial Multiplexing. Modern GPUs expose massive parallelism through hundreds of SMs, which can be logically partitioned to support multi-tenant execution. Several mechanisms have been developed to enable such partitioning. Multi-Instance GPU (MIG) (NVIDIA, 2025d) statically divides a GPU into multiple isolated instances, each with dedicated compute and memory resources. Multi-Process Service (MPS) (NVIDIA, 2025e) supports coarse-grained spatial sharing by assigning fixed groups of SMs to different processes. However, these mechanisms cannot be applied within a single process, and the overhead of reconfiguring partitions is high, making them unsuitable for dynamic and heterogeneous workload patterns. GreenContext (NVIDIA, 2025c) introduces intra-process SM partitioning by allowing different kernels or streams within the same GPU context to execute concurrently on disjoint subsets of SMs. While it can be used for on-demand spatial multiplexing, fast reconfiguration requires pre-creating multiple contexts, leading to additional memory overhead and reduced flexibility.

In contrast, our approach achieves the same goal with minimal runtime overhead by directly controlling the number of SMs available to each kernel or stream at launch time. This is enabled by `libsmctrl` (Bakita & Anderson, 2025), a recently developed low-level library that allows selectively masking SMs visible to individual kernels or streams. Operating at the driver level, `libsmctrl` provides transparent and

fine-grained control over GPU resource allocation without requiring any modification to the application or model code.

3 MOTIVATION

3.1 Existing Solutions and Room for Improvement

Chunked Prefill Limitations. Sarathi-Serve (chunked prefill) (Agrawal et al., 2024b) states that linear layers dominate the model’s forward latency in both the prefill and decode phases. Based on this observation, it proposes a token-budget-based scheduling policy in which each iteration forms a batch that fills up to a fixed number of tokens. Since linear operations are agnostic to whether tokens originate from prefill or decode requests, the total token count alone determines the computational load. Consequently, the token budget is chosen to maximize linear layer compute utilization, typically at the “knee” point of the roofline model curve, which can be obtained by profiling a linear layer’s performance on the target GPU platform.

As shown in Figure 2(a), we benchmark a linear layer of size 4096×4096 with an input dimension of $T \times 4096$, varying T (the number of tokens) to measure attainable FLOPs and latency on H100 and A100 GPUs. The results show that A100 reaches saturation around $T = 2048$, while H100 saturates near $T = 8192$. Accordingly, vLLM sets its default token budget to 2048 on A100, and increases it to 8192 on H100.

Using the token budget of 8192, we benchmark the end-to-end execution latency of the Qwen3-8B model in one iteration on an H100 GPU. Figure 2(b) presents the prefill-only batch execution latency across different batch and prompt configurations, all under a constant token budget of 8192. In all cases, the per iteration latency exceeds 180 ms. Adding a single decode request to this prefill-only batch leads the decode TBT to also exceed 180 ms. A typical TBT for decode is 100 ms (Agrawal et al., 2024b) and hence the decode will suffer a SLO violation, even though the roofline model in Figure 2(a) shows the best linear layer utilization at that token budget. Satisfying the TBT constraint, therefore, requires reducing the token budget, which lowers linear layer utilization and compromises throughput efficiency.

Observation 1: Fully consuming the token budget can violate TBT SLOs despite full linear layer utilization, while reducing the token budget improves latency at the cost of throughput efficiency.

The second trend is that the linear layer may not always dominate model latency. Since the prefill attention operation cost grows quadratically with prompt length, the attention cost cannot be controlled under a fixed token budget. As shown in Figure 2(b), although all settings use the same token budget during prefill, in the last case with a single

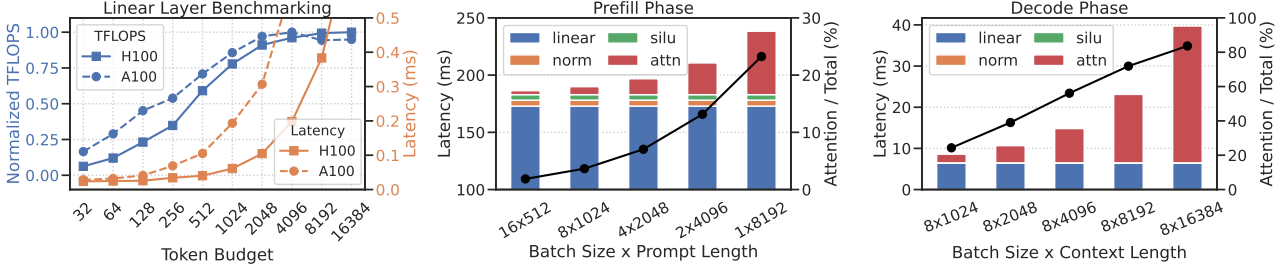


Figure 2. (a) Linear layer benchmarking shows A100 and H100 saturate near 2K and 8K tokens. (b) Prefill latency under an 8K budget violates TBT SLOs despite full utilization. (c) Decode latency rises with longer contexts as KV cache grows even under the same budget.

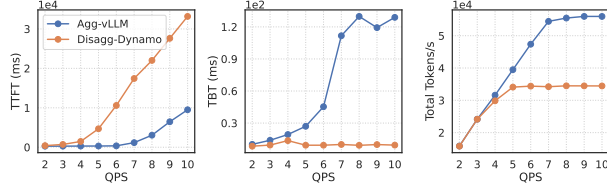


Figure 3. Performance comparison between PD aggregated and disaggregated systems across varying QPS.

8192-token prefill, the attention module accounts for approximately 25% of the total forward latency. The problem becomes more severe during the decode phase. Figure 2(c) shows profiling latency for decode-only batch execution. Although all settings use the same token budget of 8, they exhibit more than 4 \times latency variation as the context length increases. This occurs because attention latency scales with KV cache size, and KV cache reads dominate runtime as the context grows. As a result, a token-budget-based scheduler, which is derived to maximize the linear layer utilization, is sub-optimal when the context lengths increase.

Observation 2: *The token-budget-based scheduling policy ignores attention cost during both prefill and decode phases, failing to provide consistent TBT latency control.*

PD Disaggregation Limitations. We benchmark both prefill-decode (PD) aggregated with chunked prefill (Agg-vLLM) and PD disaggregated (Disagg-Dynamo) systems using Qwen3-8B on two H100 GPUs (vLLM, 2025b; NVIDIA, 2025b). In the aggregated setup, both GPUs host identical model replicas under round-robin request dispatch with a token budget of 8192. In the disaggregated setup, we adopt a 1P+1D configuration, where one GPU handles all prefill operations and the other handles decode, fully isolating the two phases. The workload consists of 8000 input tokens and 200 output tokens per request, following the official vLLM disaggregation demo (LMCache, 2025). We vary the query-per-second (QPS) rate and measure TTFT, TBT, and total token throughput.

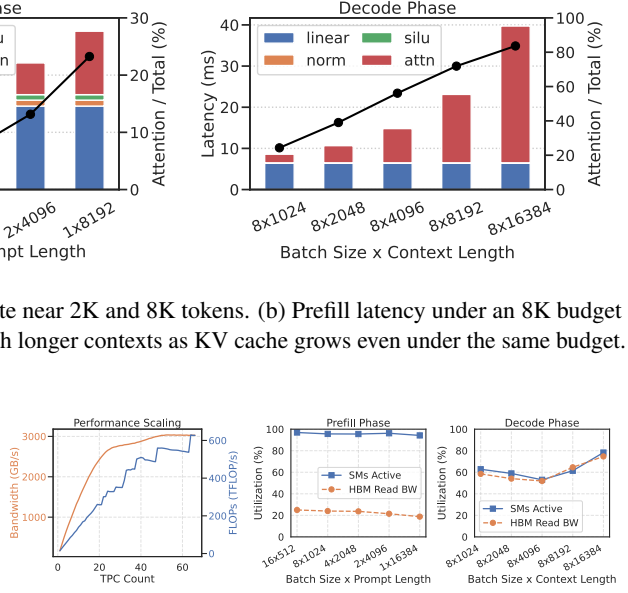


Figure 4. (a) Profiled HBM bandwidth and FLOPs versus active TPCs. (b–c) Resource utilization during prefill and decode phases.

As shown in Figure 3, although TBT remains relatively stable in the disaggregated system as QPS increases, TTFT rises sharply when QPS > 4, whereas the aggregated system starts to saturate at QPS = 7. This trend aligns with the widening throughput gap, where Disagg-Dynamo achieves less than half the total tokens per second of Agg-vLLM. The root cause is resource imbalance: in the colocated setup, both GPUs execute prefill operations concurrently, effectively doubling prefill throughput. In contrast, the disaggregated setup dedicates only one GPU to prefill, making it the system bottleneck. As QPS increases, the prefill worker's throughput lags behind that of the decode worker, resulting in overall system throughput degradation.

Observation 3: *PD disaggregated systems satisfy the TBT SLO but underutilize GPUs, reducing overall request throughput.*

3.2 Opportunity

Figure 4(a) shows the scaling of effective HBM bandwidth and FLOPs as the number of active Texture Processor Clusters (TPCs) increases on the H100 GPU. Each TPC contains two SMs and serves as the smallest unit for SM partitioning. We measure the achieved throughput using `cudaMemcpy` and `gemm` microbenchmarks. The HBM bandwidth utilization rises super-linearly with the number of active SMs; for instance, 20% of SMs already achieve approximately 60% of peak bandwidth. In contrast, FLOPs scale roughly linearly with SM count, except for minor quantization effects caused by the discrete TPC activation granularity.

Figures 4(b) and (c) compare end-to-end GPU utilization during prefill and decode. The compute-bound prefill phase saturates SM resources but leaves most HBM capacity underutilized. Conversely, the memory-bound decode phase exhibits the opposite trend: high HBM traffic with under-occupied SMs. *This complementary behavior reveals an opportunity for resource co-execution, where compute-intensive and memory-intensive workloads can share SM and HBM resources more efficiently.*

4 METHOD

Figure 1 presents an overview of DuetServe. At each iteration, the DuetServe scheduler begins with conventional chunked prefill scheduling. It first prioritizes ongoing decode requests, rescheduling them before admitting waiting prefill requests to fill the remaining token budget. If the remaining budget cannot accommodate an entire prompt, the scheduler automatically chunks the request and performs a partial prefill.

After this step, the scheduler evaluates whether the current batch risks violating the decode TBT SLO. Using the attention-aware roofline model (Section 4.1), it predicts the expected latency of the prefill-decode mixed batch. If the predicted latency exceeds the TBT bound, DuetServe proactively activates GPU spatial multiplexing (Section 4.2). The workload is then divided into two disjoint sets, a decode-only batch and a prefill-only batch, each assigned to a separate, non-overlapping SM partition for concurrent execution (Section 4.3). The core idea is to decouple decode from prefill computation, allowing decode kernels to progress independently without being blocked or synchronized at every Transformer layer.

4.1 Attention-Aware Roofline Analytical Modeling

To predict potential TBT violations and guide SM partitioning, DuetServe employs an attention-aware roofline model that estimates model forward latency based on operator, compute, and memory characteristics. Operators are categorized as token-level, sequence-level, or communication operators (Agrawal et al., 2024a).

Token-Level Operators. Token-level operators depend only on the total number of processed tokens (prefill plus decode) in the batch. These include linear projections, layer normalization, and activation functions. For the linear operator, given n total tokens, embedding dimension d , linear input dimension d_i , output dimension d_o , and element size s , the operation and memory costs are

$$F_{\text{lin}} = 2nd_i d_o, \quad B_{\text{lin}} = nd_i s + d_i d_o s + nd_o s$$

The linear operator accounts for input, output, and full weight tensor movements. This formulation applies to QKV

projection ($d_i = d_o = d$), output projection ($d_i = d_o = d$), gate-up projection ($d_i = d, d_o = m$), and down projection ($d_i = m, d_o = d$). Other token-level operators, such as layer normalization and activation functions, follow the same modeling approach with operator-specific FLOP and memory expressions. The latency of token-level operators in general is estimated as $t_{\text{tok}} = \max(F_{\text{tok}}/\Pi_{\text{SM}}, B_{\text{tok}}/\mathcal{B}_{\text{HBM}})$, where Π_{SM} denotes the compute throughput of active SMs, and \mathcal{B}_{HBM} denotes the HBM memory bandwidth.

Sequence-Level Operators. The attention operation depends on both query and key-value sequence lengths of each request within each batch. For number of attention heads h_q , key-value heads h_{kv} , and head dimension $d_h = d/h_q$, the per-request FLOPs and memory bytes are given by:

$$F_{\text{attn/req}}(q, c) = 4h_q q(q + c)d_h + 2h_q q(q + c), \\ B_{\text{attn/req}}(q, c) = 2h_q q d_h s + 2h_{kv}(q + c)d_h s,$$

where q denotes the number of scheduled query tokens and c is the number of cached key-value tokens. The first term in $F_{\text{attn/req}}$ accounts for the dominant matrix multiplication operations in query-key similarity computation and attention-value aggregation, while the second term represents element-wise softmax and scaling operations. The memory term $B_{\text{attn/req}}$ includes reads and writes for query, key, value, and output tensors.

The estimator iterates over the batch, and applies the roofline model to compute attention latency of each request and aggregate the latency:

$$t_{\text{attn}} = \sum_{r=1}^{|\mathcal{R}|} \max\left(\frac{F_{\text{attn/req}}(q_r, c_r)}{\Pi_{\text{SM}}}, \frac{B_{\text{attn/req}}(q_r, c_r)}{\mathcal{B}_{\text{SM}}}\right),$$

where $|\mathcal{R}|$ is the number of scheduled requests, and (q_r, c_r) represent the query and cached token lengths of request r .

This modelling is flexible to capture prefill ($q > 1, c = 0$), chunked prefill ($q > 1, c > 0$), and decode ($q = 1, c > 0$) attention operations for different types of requests.

Communication Operators. When scaling LLM serving across multiple GPUs within a single node, tensor parallelism is widely adopted due to its high efficiency. It requires inter-GPU communication for synchronizing the attention linear layer output u and FFN output z (Section 2). We model this communication cost using a ring AllReduce latency formulation:

$$t_{\text{allreduce}} = 2(N-1)\alpha + \frac{2(N-1)B_{\text{lin},o}}{N\mathcal{B}_{\text{NVLink}}} + \frac{N(N-1)B_{\text{lin},o}}{\Pi_{\text{SM}}},$$

where N is the number of GPUs, α is the startup latency profiled for the specific GPU platform (e.g., 3 us for H100), $B_{\text{lin},o}$ is the linear operator’s output tensor size in bytes, and

$\mathcal{B}_{\text{NVLink}}$ denotes the aggregate unidirectional bandwidth of all NVLink connections on a GPU.

The first term captures the fixed startup cost of initiating communication, including link delay and synchronization overheads; the second term models the data transfer time constrained by NVLink bandwidth; and the third term accounts for the local reduction operations performed on each GPU. This formulation reflects the $2(N - 1)$ communication rounds in a ring AllReduce protocol, consisting of a scatter-reduce phase followed by an all-gather phase, where each GPU exchanges partial results of size $B_{\text{lin},o}/N$ with its two neighbors.

Overall Estimation. DuetServe estimates Transformer block latency by summing the compute and communication costs of all sub-operations. The total model latency is then approximated as: $t_{\text{total}} = L \cdot t_{\text{block}} + t_{\text{cls}}$, where L is the number of layers and t_{cls} is the latency of the final linear classifier, modeled as a linear operator with input dimension $d_i = d$ and output dimension $d_o = \text{vocab_size}$.

4.2 GPU Partitioning Configuration Optimization

Once the roofline model predicts a TBT violation, DuetServe determines how to divide GPU resources between prefill and decode to maintain latency guarantees while maximizing overall throughput.

At initialization, DuetServe profiles the achievable compute throughput $\Pi_{\text{SM}}(S)$ and memory bandwidth $\mathcal{B}_{\text{HBM}}(S)$ for each possible SM partition size S . For a candidate split assigning S_d SMs to decode and $S_p = S - S_d$ SMs to prefill, the predicted latencies follow the roofline model:

$$t_p(S_p) = f_{\text{roofline}}(\mathcal{R}_{\text{prefill}}, \Pi_{\text{SM}}(S_p), \mathcal{B}_{\text{HBM}}(S_p)),$$

$$t_d(S_d) = f_{\text{roofline}}(\mathcal{R}_{\text{decode}}, \Pi_{\text{SM}}(S_d), \mathcal{B}_{\text{HBM}}(S_d)).$$

When proactive SM partitioning is triggered, the decode TBT SLO is already at risk of violation, and the system typically operates in the regime where $t_p(S_p) > t_d(S_d)$. To mitigate idle periods and balance utilization, we execute k decode steps on S_d SMs while one prefill batch runs concurrently on S_p SMs. The total latency of such a configuration is expressed as:

$$t(S_p, S_d, k) = \max(k t_d(S_d), t_p(S_p)),$$

which indicates that residual compute bubbles may still occur on either the decode or prefill side, depending on the chosen configuration.

Let T_{decode} denote the number of tokens produced per decode step across the scheduled decode requests, and T_{prefill} denote the number of tokens in the scheduled prefill batch.

Algorithm 1 DuetServe Scheduling Algorithm

```

1: Input: Scheduled prefill and decode requests  $\mathcal{R}_{\text{mixed}}$ ,  

   TBT SLO  $\tau_{\text{TBT}}$ , total SMs count  $S$ 
2:  $t_{\text{mixed}}(S) = f_{\text{roofline}}(\mathcal{R}_{\text{mixed}}, \Pi_{\text{SM}}(S), \mathcal{B}_{\text{HBM}}(S))$ 
3: if  $t_{\text{mixed}}(S) \leq \tau_{\text{TBT}}$  then
4:   GPU_temporal_sharing_execute( $\mathcal{R}_{\text{mixed}}, S$ )
5: else
6:    $\mathcal{R}_{\text{prefill}}, \mathcal{R}_{\text{decode}} \leftarrow \mathcal{R}_{\text{mixed}}$ 
7:    $\rho^* \leftarrow 0, \mathcal{C}^* \leftarrow \emptyset$ 
8:   for  $S_d$  in range(1,  $S + 1, 2$ ) do
9:      $t_d(S_d) = f_{\text{roofline}}(\mathcal{R}_{\text{decode}}, \Pi_{\text{SM}}(S_d), \mathcal{B}_{\text{HBM}}(S_d))$ 
10:    if  $t_d(S_d) > \tau_{\text{TBT}}$  then
11:      continue
12:    end if
13:     $S_p \leftarrow S - S_d$ 
14:     $t_p(S_p) = f_{\text{roofline}}(\mathcal{R}_{\text{prefill}}, \Pi_{\text{SM}}(S_p), \mathcal{B}_{\text{HBM}}(S_p))$ 
15:    for  $k$  in  $(\lfloor \frac{t_p(S_p)}{t_d(S_d)} \rfloor, \lfloor \frac{t_p(S_p)}{t_d(S_d)} \rfloor + 1)$  do
16:       $\rho \leftarrow \frac{k T_{\text{decode}} + T_{\text{prefill}}}{\max(k t_d(S_d), t_p(S_p))}$ 
17:      if  $\rho > \rho^*$  then
18:         $\rho^* \leftarrow \rho, \mathcal{C}^* \leftarrow (S_p, S_d, k)$ 
19:      end if
20:    end for
21:  end for
22:  GPU_spatial_sharing_execute( $\mathcal{R}_{\text{prefill}}, \mathcal{R}_{\text{decode}}, \mathcal{C}^*$ )
23: end if

```

The scheduler seeks the configuration (S_p, S_d, k) that maximizes total token throughput under the latency constraint:

$$\max_{S_p, S_d, k} \frac{k T_{\text{decode}} + T_{\text{prefill}}}{\max(k t_d(S_d), t_p(S_p))}$$

$$\text{s.t. } t_d(S_d) \leq \tau_{\text{TBT}},$$

where τ_{TBT} is the predefined TBT latency bound.

Note that this optimization naturally favors allocating more SMs to the prefill task to reduce its latency while assigning the minimal SMs required for decode to just satisfy the TBT constraint, since prefill contributes more substantially to total throughput. In practice, the scheduler enumerates feasible values of S_d , discards configurations violating the TBT constraint, and calculates the throughput of each configuration to solve the optimization problem with negligible CPU overhead.

4.3 Interruption-Free Kernel Dispatching and Look-Ahead Decode Execution

To enable concurrent prefill and decode execution, DuetServe initializes two dedicated CUDA streams, one for decode and one for prefill. After determining the optimal SM partitioning configuration, the scheduler invokes `libsmtctrl` to bind each stream to its designated SM re-

gion, ensuring that the two workloads execute independently without interference. GPU kernels for both batches are then dispatched concurrently by the CPU within their respective stream contexts.

To minimize CPU-side dispatch overhead, DuetServe leverages CUDA Graph capture for decode execution. During initialization, the system records the sequence of decode kernels into a reusable CUDA Graph (NVIDIA, 2025a), enabling efficient graph replay with negligible launch latency. Prefill execution, however, cannot be similarly captured because its attention kernels often exhibit dynamic tensor shapes and variable control flows (vLLM, 2025a). Consequently, prefill kernels are launched individually by the CPU, while decode kernels are launched collectively through the cached CUDA Graph. Since launching a CUDA Graph introduces less than 0.5 ms of overhead, compared to tens of milliseconds for prefill kernel dispatch, the scheduler always initiates decode execution first to prevent CPU-induced stalls, as shown in Figure 5.

To further reduce synchronization overhead between consecutive decode steps, DuetServe introduces a look-ahead decode execution mechanism. In conventional decoding, each iteration involves CPU-side synchronization to sample tokens, filter completed requests, update KV cache mappings, and prepare input metadata for the next step. These operations create frequent CPU–GPU stalls that limit overlap with prefill. The look-ahead strategy eliminates these interruptions by preallocating multiple KV cache slots per request and preparing all metadata for k future decode steps in advance. The CPU then launches k pre-recorded CUDA Graphs consecutively without waiting for intermediate synchronization, allowing continuous GPU execution across multiple decode iterations.

5 EVALUATION

5.1 Experimental Setup

Testbed. Experiments are conducted on a server equipped with a 96-core Intel Xeon Platinum 8480C CPU and two NVIDIA H100 GPUs (80 GB) connected via NVLink, running driver version 580.95.05 and CUDA 13.0. All experiments are conducted using PyTorch 2.8.0.

Implementation. We implement DuetServe from scratch with approximately 3,000 lines of Python code. The system integrates the `libsmctr1` CUDA library through a Python API to control GPU SM allocation per CUDA stream. It incorporates essential online serving optimizations, including paged KV cache management (Kwon et al., 2023), continuous batching (Yu et al., 2022), CUDA Graph capture and replay (NVIDIA, 2025a), `torch.compile` kernel fusion (PyTorch, 2025), and the FlashAttention-3 kernel (Shah et al., 2024). Tensor parallel inference is implemented using

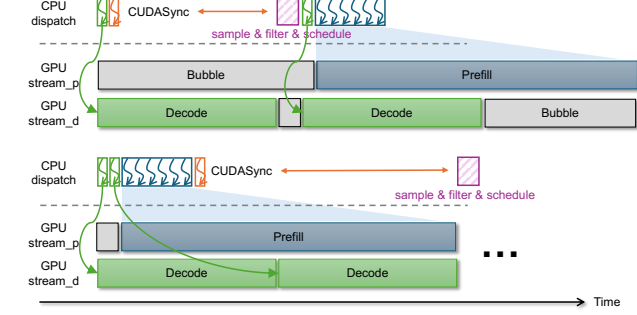


Figure 5. (Top) Conventional decoding incurs CPU–GPU stalls from per-step synchronization. (Bottom) Interruption-free kernel dispatching by scheduling multiple decoding steps in advance.

Table 1. Workload traces used for evaluations.

TRACE	# REQUESTS	ISL	OSL
AZURE-CODE	19366	2047	28
AZURE-CONV	8819	1155	211
MOONCAKE	1000	12035	343

NCCL to handle inter-GPU communication.

Models and Workloads. We evaluate two representative LLMs: Qwen3-8B (TP = 1) and Qwen3-14B (TP = 2). Three real-world LLM serving traces are used as workloads: Azure Code (Microsoft, 2023), Azure Conversation (Microsoft, 2023), and Mooncake Conversation (Qin et al., 2025). These traces exhibit distinct usage patterns and token length distributions, summarized in Table 1. For Mooncake Conversation, we sample 1,000 requests due to the trace’s large scale. Following prior work (Yu et al., 2022; Kwon et al., 2023), we model request arrivals using a Poisson process to simulate realistic serving dynamics.

Baselines. We compare DuetServe with four state-of-the-art LLM serving systems under both PD aggregation and PD disaggregation settings:

- vLLM (v0.10.1-v1): employs the default chunked prefill scheduler with a token budget of 8192 on H100.
- SGLang-Default (v0.5.0): employs a throughput-oriented scheduler that opportunistically executes prefill-only batches when sufficient GPU memory is available for several consecutive iterations, before switching to decode-only iterations to drain pending requests.
- SGLang-Chunked: configured with serving argument `enable-mixed-chunk` to enable the Sarathi-Serve chunked-prefill scheduler, using a token budget of 8192.
- Dynamo (v0.5.1) with vLLM backend: implements PD disaggregation in a 2-GPU setup, assigning one GPU to the prefill phase (1P) and the other to the decode phase (1D). KV cache transfer is managed via the NIXL library, optimized for P2P GPU communication.

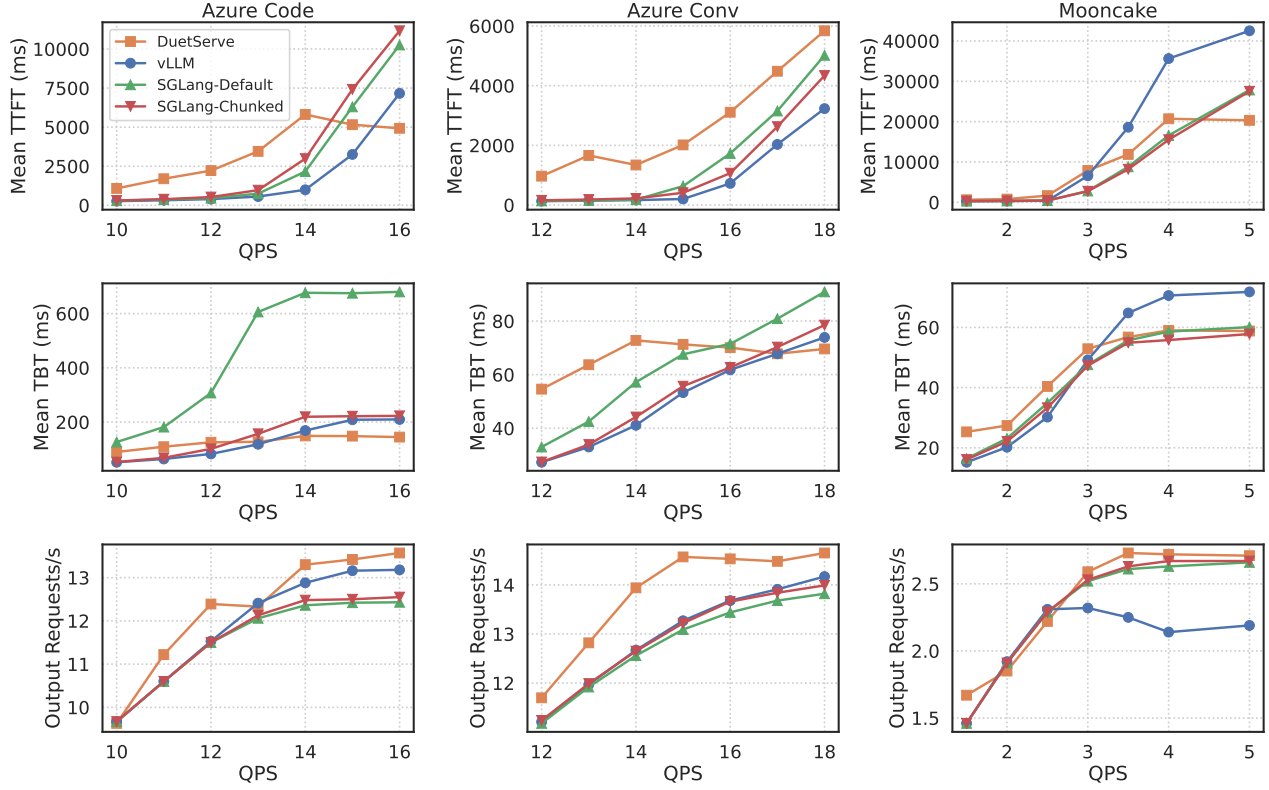


Figure 6. The end-to-end performance of difference workloads with Qwen3-8B.

All baselines employ consistent configurations for fair comparison: a maximum batch size of 1024, a GPU memory utilization ratio of 0.9, and FlashAttention-3 (Shah et al., 2024) as the attention backend.

Metrics. We report three key metrics: mean TTFT, mean TBT, and output request throughput. Throughput is defined as the total number of completed requests divided by the end-to-end serving duration, indicating the system’s maximum serving capacity. An efficient serving system should achieve low latency while sustaining high throughput under increasing request loads.

5.2 End-to-end Performance

As shown in Figure 6, across the three workloads using Qwen3-8B (TP = 1), DuetServe consistently achieves the lowest TBT and highest output request throughput. In Azure-Code, DuetServe maintains TBT below 150 ms at QPS = 16, whereas both vLLM and SGLang-Chunked exceed 200 ms. Notably, the SGLang-Default baseline exhibits unbounded TBT growth, surpassing 680 ms, as it repeatedly inserts prefill-only batches that interrupt decode generations. By prioritizing decode progress and executing prefill concurrently, DuetServe (13.57 req/s) achieves 1.1× higher throughput than SGLang-Default (12.43 req/s)

at QPS = 16. Although DuetServe’s TTFT is slightly higher at light load, this reflects an intentional design tradeoff: the system safeguards the decode TBT SLO while opportunistically advancing prefill using leftover GPU resources. Prefill latency, and consequently TTFT, can be relaxed under light workloads to favor decode responsiveness, improving steady-state throughput. Hence, modest TTFT fluctuations indicate that the GPU is fully utilized rather than inefficiently scheduled.

In Azure-Conv and Mooncake workloads, the same pattern persists. DuetServe bounds TTFT growth even beyond QPS = 15 and 3, respectively, demonstrating stronger queue stability and balanced SM utilization. More importantly, its TBT remains consistently lower than both vLLM and SGLang, achieving up to 1.3x higher output request throughput than vLLM at peak load in Mooncake. Specifically, vLLM reaches 2.14 requests/s, while DuetServe sustains 2.72 requests/s at QPS = 5. This improvement stems from DuetServe’s ability to execute decode steps independently of prefill synchronization, allowing requests to complete faster. While vLLM achieves the lowest TTFT at light load, DuetServe’s higher throughput and stable TBT under contention underscore its effectiveness in sustaining low-latency token generation under full GPU saturation.

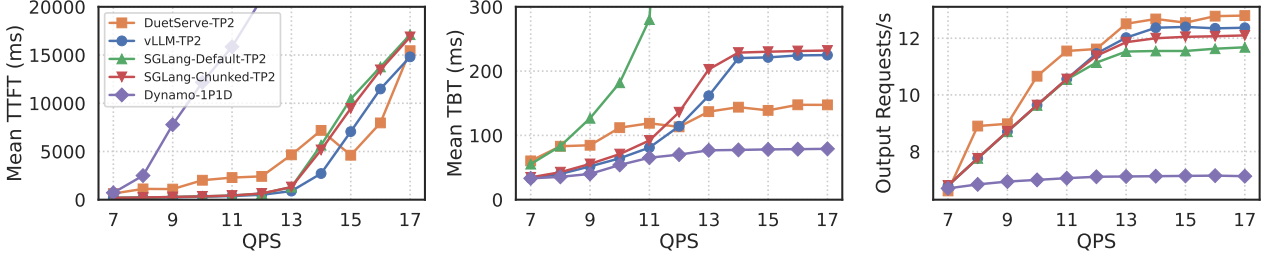


Figure 7. The end-to-end performance of Azure-Code workload with Qwen3-14B (TP = 2).

5.3 Multi-GPU Inference Performance

We extend the experiments to a multi-GPU environment. In the PD aggregated setting, we adopt a tensor parallelism (TP) degree of 2, evenly splitting model weights across two GPUs. Both vLLM and SGLang baselines use the same TP configuration for fair comparison. In the PD disaggregated setting, Dynamo assigns one GPU as the prefill worker and another as the decode worker (1P+1D).

As shown in Figure 7, DuetServe-TP2 achieves the second-lowest TBT while maintaining the highest throughput across all QPS levels. While vLLM-TP2 and SGLang-Chunked-TP2 exhibit rising TBT beyond 200 ms once QPS exceeds 13, DuetServe sustains stable per-token latency below 150 ms even under saturation. The SGLang-Default-TP2 baseline again suffers from unbounded TBT growth due to frequent prefill interruptions, whereas Dynamo-1P1D achieves the lowest TBT but at the expense of throughput. Its prefill GPU becomes the bottleneck, leaving the decode GPU underutilized because its throughput cannot keep pace with the decode stage. Overall, these results confirm that DuetServe’s adaptive spatial multiplexing scales effectively under multi-GPU execution, maintaining low decoding latency while avoiding the inefficiency and imbalance inherent in fully disaggregated PD configurations.

5.4 Ablation Study

Roofline Modeling Accuracy. Figure 8 compares the profiled latency with the latency estimated by the roofline analytical model for both the 8×1024 prefill and 16×1024 decode workloads on Qwen3-8B (TP = 1) and Qwen3-14B (TP = 2). For the compute-bound prefill phase, the model tracks the measured latency closely across different TPC counts, showing nearly linear latency reduction until about 40 TPCs, after which the curve flattens as compute throughput saturates. This confirms that prefill latency is dominated by SM compute utilization rather than memory bandwidth. In contrast, the decode phase exhibits limited scalability: latency quickly plateaus once a small number of TPCs are active. The analytical estimates slightly overpredict latency

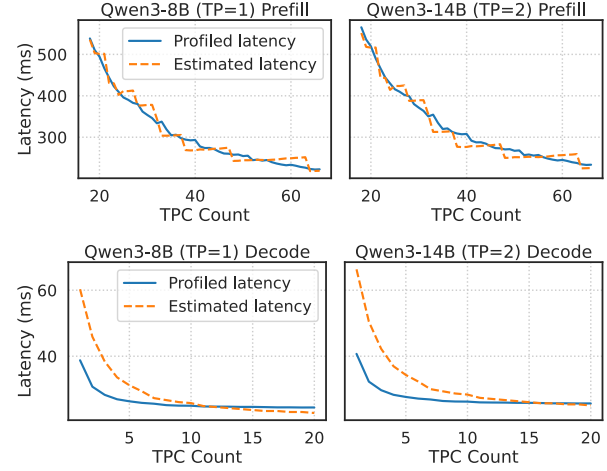


Figure 8. Profiled and roofline-modeled latency comparison.

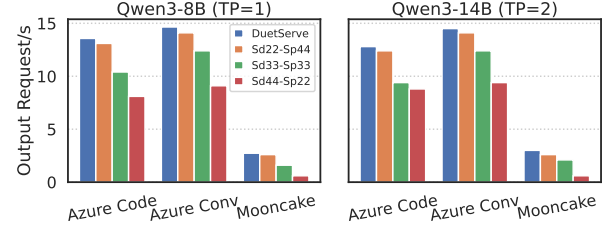


Figure 9. Throughput comparison across workloads and models using static SM partitioning versus DuetServe.

in the decode case, but still capture the overall scaling trend. Together, these results validate the roofline model’s accuracy for modeling latency under different workloads and SM counts.

Static SM Partitioning. Figure 9 compares system throughput under different static SM partitioning ratios for Qwen3-8B (TP = 1) and Qwen3-14B (TP = 2) across the Azure-Code, Azure-Conv, and Mooncake workloads. The three configurations Sd22-Sp44, Sd33-Sp33, and Sd44-Sp22 represent fixed SM allocations between the decode and prefill phases. Throughput varies noticeably



Figure 10. Profiled CPU and GPU activities showing DuetServe’s concurrent prefill and decode execution.

across workloads, confirming that static partitioning leads to persistent imbalance: either idle compute resources in one phase or congestion in the other. In contrast, DuetServe’s adaptive scheduling dynamically reallocates SMs at runtime, maintaining balanced utilization and higher concurrency under diverse traffic conditions.

Latency Breakdown. Figure 10 shows CPU and GPU activities and SM utilization over two consecutive iterations during LLM serving. In the first iteration, the scheduler assigns 48 TPCs to the prefill stream and 18 TPCs to the decode stream, running five decode steps before synchronizing with prefill execution. The CPU scheduling overhead, including solving the optimal GPU partitioning configuration, remains below 1 ms. Decode kernels are launched first, causing a short delay before prefill execution begins, but both streams sustain high overlap and stable SM efficiency. In the second iteration, the execution switches back to PD mixed mode on the main stream, where prefill and decode requests execute synchronously in a unified context. This transition highlights DuetServe’s adaptive scheduler, which alternates between spatial and temporal sharing based on workload characteristics and predicted latency.

6 RELATED WORKS

LLM Serving Frameworks. Early LLM serving systems focused on unified execution to improve throughput and memory efficiency. ORCA (Yu et al., 2022) introduced continuous batching to reduce request latency and improve GPU utilization. FastServe (Wu et al., 2023) later challenged the standard first-come, first-served policy, proposing priority-based scheduling to reduce average request latency. vLLM (Kwon et al., 2023) addressed KV cache memory fragmentation via PagedAttention, by dividing memory space into blocks and allocating them to requests on demand. SGLang (Zheng et al., 2024) proposed RadixAttention to maximize KV reuse across multi-turn generations. Sarathi-Serve (Agrawal et al., 2024b) improved efficiency through chunked prefill and reduced pipeline bubbles.

GPU Resource Sharing. GPU resource sharing focuses on efficient allocation among multiple ML workloads. GSLICE (Dhakal et al., 2020) and KRISP (Chow et al., 2023) apply spatial partitioning to colocate tasks, while Orion (Strati et al., 2024), REEF (Han et al., 2022), and BLESS (Zhang et al., 2025) leverage fine-grained tempo-

ral multiplexing for DNN inference. However, these target general ML workloads, not LLM-specific needs. MuxServe (Duan et al., 2024) addresses this gap by combining spatial and temporal sharing to colocate multiple LLMs, allocating separate GPU resources to prefill and decode. Drift (Cui et al., 2025) partitions SMs statically for concurrent execution of prefill and decode phases, whereas Bullet (Lin et al., 2025) and Semi-PD (Hong et al., 2025) dynamically adapt SM allocation using feedback loops and latency models. Nexus (Shi et al., 2025) further optimizes GPU spatial sharing with a runtime KV-aware analytical model. At the kernel level, NanoFlow (Zhu et al., 2025) overlaps compute, memory, and network operations, while POD-Attention (Kamath et al., 2025) fuses prefill and decode attention kernels into a single one to maximize SM utilization.

PD Disaggregated Systems. To reduce phase interference, recent systems decouple prefill and decode across heterogeneous hardware. DistServe (Zhong et al., 2024) assigns each phase to separate GPUs and searches for optimal model-parallel strategies per phase. Splitwise (Patel et al., 2024) explores both homogeneous and heterogeneous device configurations to optimize cost, throughput, and power efficiency. TetriInfer (Hu et al., 2024b) employs a two-level scheduling algorithm with resource prediction to balance load across GPUs. Mooncake (Qin et al., 2025) and MemServe (Hu et al., 2024a) introduce distributed KV cache memory pools to enable cache reuse, while Wind-Serve (Feng et al., 2025) reduces GPU underutilization through stream-based dynamic rescheduling across prefill and decode instances. Dynamo (NVIDIA, 2025b) further proposes KV-aware request routing and multi-level memory KV cache offloading. Although these approaches effectively mitigate phase interference and improve efficiency, they introduce higher system complexity through cross-instance orchestration and KV cache transfer overhead, and remain less adaptive to dynamic input traffic patterns.

7 CONCLUSION

This work presented DuetServe, an adaptive LLM serving framework that unifies the benefits of aggregated and disaggregated execution. By predicting contention with an attention-aware roofline model and activating fine-grained SM-level partitioning when needed, DuetServe enables concurrent prefill and decode execution within a single GPU, improving throughput while preserving latency SLOs.

REFERENCES

Agrawal, A., Kedia, N., Mohan, J., Panwar, A., Kwatra, N., Gulavani, B. S., Ramjee, R., and Tumanov, A. Vidur: A large-scale simulation framework for llm inference. In Gibbons, P., Pekhimenko, G., and Sa, C. D. (eds.), *Proceedings of Machine Learning and Systems*, volume 6, pp. 351–366, 2024a.

Agrawal, A., Kedia, N., Panwar, A., Mohan, J., Kwatra, N., Gulavani, B., Tumanov, A., and Ramjee, R. Taming throughput-latency tradeoff in llm inference with sarathi-serve. In *18th USENIX Symposium on Operating Systems Design and Implementation (OSDI 24)*, pp. 117–134, 2024b.

Bakita, J. and Anderson, J. H. Hardware compute partitioning on nvidia gpus for composable systems. In *37th Euromicro Conference on Real-Time Systems (ECRTS 2025)*, 2025. URL <https://drops.dagstuhl.de/entities/document/10.4230/LIPIcs.ECRTS.2025.21>.

Chow, M., Jahanshahi, A., and Wong, D. Krisp: Enabling kernel-wise right-sizing for spatial partitioned gpu inference servers. In *Proceedings of the 29th IEEE International Symposium on High Performance Computer Architecture (HPCA)*, 2023.

Cui, W., Chen, Y., Zhao, H., Xu, Z., Chen, Q., Chen, X., Zhou, Y., Sun, S., and Guo, M. Optimizing slo-oriented llm serving with pd-multiplexing. *arXiv preprint arXiv:2504.14489*, 2025.

Dao, T., Fu, D., Ermon, S., Rudra, A., and Ré, C. Flashattention: Fast and memory-efficient exact attention with io-awareness. In Koyejo, S., Mohamed, S., Agarwal, A., Belgrave, D., Cho, K., and Oh, A. (eds.), *Advances in Neural Information Processing Systems*, volume 35, pp. 16344–16359. Curran Associates, Inc., 2022.

Dhakal, A., Kulkarni, S. G., and Ramakrishnan, K. K. Gslice: controlled spatial sharing of gpus for a scalable inference platform. In *Proceedings of the 11th ACM Symposium on Cloud Computing, SoCC ’20*, pp. 492–506, New York, NY, USA, 2020. Association for Computing Machinery. ISBN 9781450381376. doi: 10.1145/3419111.3421284.

Duan, J., Lu, R., Duanmu, H., Li, X., Zhang, X., Lin, D., Stoica, I., and Zhang, H. Muxserve: Flexible spatial-temporal multiplexing for multiple llm serving. *arXiv preprint arXiv:2404.02015*, 2024.

Feng, J., Huang, Y., Zhang, R., Liang, S., Yan, M., and Wu, J. Windserve: Efficient phase-disaggregated llm serving with stream-based dynamic scheduling. In *Proceedings of the 52nd Annual International Symposium on Computer Architecture, ISCA ’25*, pp. 1283–1295, New York, NY, USA, 2025. Association for Computing Machinery. ISBN 9798400712616. doi: 10.1145/3695053.3730999.

Gemini-Team, Anil, R., Borgeaud, S., Alayrac, J.-B., Yu, J., Soricut, R., Schalkwyk, J., Dai, A. M., Hauth, A., Millican, K., Silver, D., and et al. Gemini: A family of highly capable multimodal models, 2024. URL <https://arxiv.org/abs/2312.11805>.

Grattafiori, A., Dubey, A., Jauhri, A., Pandey, A., Kadian, A., Al-Dahle, A., Letman, A., Mathur, A., Schelten, A., Vaughan, A., Yang, A., Fan, A., Goyal, A., Hartshorn, A., Yang, A., Mitra, A., Srivankumar, A., Korenev, A., Hinsvark, A., Rao, A., Zhang, A., and et al. The llama 3 herd of models, 2024. URL <https://arxiv.org/abs/2407.21783>.

Han, M., Zhang, H., Chen, R., and Chen, H. Microsecond-scale preemption for concurrent gpu-accelerated dnn inferences. In *16th USENIX Symposium on Operating Systems Design and Implementation (OSDI 22)*, pp. 539–558, 2022.

Hong, K., Chen, L., Wang, Z., Li, X., Mao, Q., Ma, J., Xiong, C., Wu, G., Han, B., Dai, G., et al. semi-pd: Towards efficient llm serving via phase-wise disaggregated computation and unified storage. *arXiv preprint arXiv:2504.19867*, 2025.

Hu, C., Huang, H., Hu, J., Xu, J., Chen, X., Xie, T., Wang, C., Wang, S., Bao, Y., Sun, N., and Shan, Y. Memserve: Context caching for disaggregated llm serving with elastic memory pool, 2024a. URL <https://arxiv.org/abs/2406.17565>.

Hu, C., Huang, H., Xu, L., Chen, X., Xu, J., Chen, S., Feng, H., Wang, C., Wang, S., Bao, Y., et al. Inference without interference: Disaggregate llm inference for mixed downstream workloads. *arXiv preprint arXiv:2401.11181*, 2024b.

Kamath, A. K., Prabhu, R., Mohan, J., Peter, S., Ramjee, R., and Panwar, A. Pod-attention: Unlocking full prefill-decode overlap for faster llm inference. In *Proceedings of the 30th ACM International Conference on Architectural Support for Programming Languages and Operating Systems, Volume 2*, pp. 897–912, 2025.

Kwon, W., Li, Z., Zhuang, S., Sheng, Y., Zheng, L., Yu, C. H., Gonzalez, J., Zhang, H., and Stoica, I. Efficient memory management for large language model serving with pagedattention. In *Proceedings of the 29th symposium on operating systems principles*, pp. 611–626, 2023.

Li, G., Hammoud, H. A. A. K., Itani, H., Khizbulin, D., and Ghanem, B. Camel: Communicative agents for "mind" exploration of large language model society. In *Thirty-seventh Conference on Neural Information Processing Systems*, 2023.

Lin, Z., Xu, H., Chen, G., Zhang, X., and Lu, Y. Bullet: Boosting gpu utilization for llm serving via dynamic spatial-temporal orchestration. *arXiv preprint arXiv:2504.19516*, 2025.

Liu, Y., Zhang, K., Li, Y., Yan, Z., Gao, C., Chen, R., Yuan, Z., Huang, Y., Sun, H., Gao, J., He, L., and Sun, L. Sora: A review on background, technology, limitations, and opportunities of large vision models, 2024. URL <https://arxiv.org/abs/2402.17177>.

LMCache. Bringing state-of-the-art pd speed to vllm v1 with lmcache, April 29 2025. URL <https://blog.lmcache.ai/2025-04-29-pdbench/>. Accessed: 2025-10-29.

Luo, J., Zhang, W., Yuan, Y., Zhao, Y., Yang, J., Gu, Y., Wu, B., Chen, B., Qiao, Z., Long, Q., Tu, R., Luo, X., Ju, W., Xiao, Z., Wang, Y., Xiao, M., Liu, C., Yuan, J., Zhang, S., Jin, Y., Zhang, F., Wu, X., Zhao, H., Tao, D., Yu, P. S., and Zhang, M. Large language model agent: A survey on methodology, applications and challenges, 2025.

Microsoft. Azure llm inference trace 2023, 2023. URL <https://github.com/Azure/AzurePublicDataset/blob/master/AzureLLMInferenceDataset2023.md>.

NVIDIA. Cuda runtime api: Graph management, 2025a. URL https://docs.nvidia.com/cuda/cuda-runtime-api/group__CUDART__GRAPH.html. Accessed: 2025-10-29.

NVIDIA. Nvidia dynamo – a low-latency distributed inference framework, 2025b. URL <https://developer.nvidia.com/dynamo>. Accessed: 2025-10-29.

NVIDIA. Green contexts - cuda driver api, 2025c. URL https://docs.nvidia.com/cuda/cuda-driver-api/group__CUDA__GREEN__CONTEXTS.html. Accessed: 2025-10-29.

NVIDIA. Multi-instance gpu (mig), 2025d. URL <https://www.nvidia.com/en-us/technologies/multi-instance-gpu/>. Accessed: 2025-10-29.

NVIDIA. Multi-process service (mps), 2025e. URL <https://docs.nvidia.com/deploy/mps/index.html>. Accessed: 2025-10-29.

OpenAI, Achiam, J., Adler, S., Agarwal, S., Ahmad, L., Akkaya, I., Aleman, F. L., Almeida, D., Altenschmidt, J., Altman, S., Anadkat, S., Avila, R., Babuschkin, I., Balaji, S., Balcom, V., and et al. Gpt-4 technical report, 2024a. URL <https://arxiv.org/abs/2303.08774>.

OpenAI, Hurst, A., Lerer, A., Goucher, A. P., Perelman, A., Ramesh, A., Clark, A., Ostrow, A., Welihinda, A., Hayes, A., Radford, A., Madry, A., Baker-Whitcomb, A., Beutel, A., Borzunov, A., Carney, A., Chow, A., Kirillov, A., Nichol, A., Paino, A., Renzin, A., Passos, A. T., and et al. Gpt-4o system card, 2024b. URL <https://arxiv.org/abs/2410.21276>.

Patel, P., Choukse, E., Zhang, C., Shah, A., Goiri, I., Maleki, S., and Bianchini, R. Splitwise: Efficient generative llm inference using phase splitting. In *2024 ACM/IEEE 51st Annual International Symposium on Computer Architecture (ISCA)*, pp. 118–132. IEEE, 2024.

PyTorch. Introduction to `torch.compile`, 2025. URL https://docs.pytorch.org/tutorials/intermediate/torch_compile_tutorial.html. Accessed: 2025-10-29.

Qin, R., Li, Z., He, W., Cui, J., Ren, F., Zhang, M., Wu, Y., Zheng, W., and Xu, X. Mooncake: Trading more storage for less computation—a kvcache-centric architecture for serving llm chatbot. In *23rd USENIX Conference on File and Storage Technologies (FAST 25)*, pp. 155–170, 2025.

Shah, J., Bikshandi, G., Zhang, Y., Thakkar, V., Ramani, P., and Dao, T. Flashattention-3: Fast and accurate attention with asynchrony and low-precision. In *The Thirty-eighth Annual Conference on Neural Information Processing Systems*, 2024. URL <https://openreview.net/forum?id=tVConYid20>.

Shi, X., Cai, C., Du, J., and Jia, Z. Nexus: Proactive intra-gpu disaggregation of prefill and decode in llm serving. *arXiv preprint arXiv:2507.06608*, 2025.

Strati, F., Ma, X., and Klimovic, A. Orion: Interference-aware, fine-grained gpu sharing for ml applications. In *Proceedings of the Nineteenth European Conference on Computer Systems*, pp. 1075–1092, 2024.

vLLM. Cuda graphs compatibility of attention backends, 2025a. URL https://docs.vllm.ai/en/latest/design/cuda_graphs.html. Accessed: 2025-10-29.

vLLM. vllm: A high-throughput and memory-efficient library for llm inference and serving. <https://github.com/vllm-project/vllm>, 2025b. Accessed: 2025-10-29.

Wu, B., Zhong, Y., Zhang, Z., Huang, G., Liu, X., and Jin, X. Fast distributed inference serving for large language models, 2023.

Yang, A., Li, A., Yang, B., Zhang, B., Hui, B., Zheng, B., Yu, B., Gao, C., Huang, C., Lv, C., Zheng, C., Liu, D., Zhou, F., Huang, F., Hu, F., Ge, H., Wei, H., Lin, H., Tang, J., Yang, J., Tu, J., and et al. Qwen3 technical report, 2025. URL <https://arxiv.org/abs/2505.09388>.

Yu, G.-I., Jeong, J. S., Kim, G.-W., Kim, S., and Chun, B.-G. Orca: A distributed serving system for transformer-based generative models. In *16th USENIX Symposium on Operating Systems Design and Implementation (OSDI 22)*, pp. 521–538, 2022.

Zhang, S., Chen, Q., Cui, W., Zhao, H., Xue, C., Zheng, Z., Lin, W., and Guo, M. Improving gpu sharing performance through adaptive bubbleless spatial-temporal sharing. In *Proceedings of the Twentieth European Conference on Computer Systems*, pp. 573–588, 2025.

Zheng, L., Yin, L., Xie, Z., Sun, C. L., Huang, J., Yu, C. H., Cao, S., Kozyrakis, C., Stoica, I., Gonzalez, J. E., et al. Sqlang: Efficient execution of structured language model programs. *Advances in neural information processing systems*, 37:62557–62583, 2024.

Zhong, Y., Liu, S., Chen, J., Hu, J., Zhu, Y., Liu, X., Jin, X., and Zhang, H. Distserve: Disaggregating prefill and decoding for goodput-optimized large language model serving. In *18th USENIX Symposium on Operating Systems Design and Implementation (OSDI 24)*, pp. 193–210, 2024.

Zhu, K., Gao, Y., Zhao, Y., Zhao, L., Zuo, G., Gu, Y., Xie, D., Ye, Z., Kamahori, K., Lin, C.-Y., et al. Nanoflow: Towards optimal large language model serving throughput. In *19th USENIX Symposium on Operating Systems Design and Implementation (OSDI 25)*, pp. 749–765, 2025.